Experimental Characterization of the Electron Heat Transport in Low-Density ASDEX Upgrade Plasmas

F. Ryter,[1] F. Imbeaux,[2] F. Leuterer,[1] H.-U. Fahrbach,[1] W. Suttrop,[1] and ASDEX Upgrade Team[1]
[1]*Max-Planck-Institut für Plasmaphysik, EURATOM Association, D-85748 Garching, Germany*
[2]*Département de Recherches sur la Fusion Contrôlée, Association Euratom–CEA, CEA Cadarache, 13108 St. Paul lez Durance Cedex, France*
(Received 11 December 2000)

The electron heat transport is investigated in ASDEX Upgrade conventional L-mode plasmas with pure electron heating provided by electron-cyclotron heating (ECH) at low density. Under these conditions, steady-state and ECH modulation experiments indicate without ambiguity that electron heat transport exhibits a clear threshold in $\nabla T_e/T_e$ and also suggest that it has a gyro-Bohm character.

DOI: 10.1103/PhysRevLett.86.5498 PACS numbers: 52.55.Fa, 52.25.Fi

For the last two decades the electron temperature profiles in tokamak plasmas were observed to react weakly to changes of the auxiliary heating deposition profile, as described in [1–6] and more recently [7–9]. This property, known as "profile resilience" or "profile stiffness," can be provided by a strong increase of transport when the electron temperature profile T_e exceeds a threshold in ∇T_e or $\nabla T_e/T_e$. In addition, the high value of the experimental electron heat conductivity, as compared to neoclassical theory, is attributed to microturbulence. Two sources of turbulence appear to be good candidates to explain electron transport in tokamak plasmas: the trapped electron modes (TEM) and the electron temperature gradient (ETG) driven modes. The TEMs have been well established for several years [10–12], and, in conjunction with the ion temperature gradient modes, seem to explain transport in plasmas with $T_e \approx T_i$ and comparable ion and electron heating [13]. In contrast, it was believed that turbulence driven by ETG would not be able to drive a large transport, due to the very small size of the turbulence cells. New nonlinear calculations indicate that the turbulence cells can indeed become much larger, building so-called "streamers" with a large radial extension and therefore able to cause a large transport [14,15]. Both ETG (with associated streamers) and collisionless TEM driven turbulence have a threshold $(\nabla T_e/T_e)_c$ and are possible candidates to explain the electron heat transport and the observed profile stiffness. Above the threshold, transport increases strongly, which tends to keep the T_e profiles close to $(\nabla T_e/T_e)_c$. In the cases where they are effectively limited by $(\nabla T_e/T_e)_c$, the T_e profiles have the same shape and, plotted on a logarithmic scale, are just shifted with respect to each other according to the boundary condition which is the temperature in the plasma edge region. A simple model for the heat diffusivity χ_e determined by temperature gradient (TG) driven turbulence can be written as:

$$\chi_e = T_e^{3/2}\{\xi_0 + \xi_{TG} \cdot \mathcal{G}[\nabla T_e/T_e - (\nabla T_e/T_e)_c]\}, \quad (1)$$

where ξ_0 describes transport in the absence of TG modes and $\xi_{\mathrm{TG}} \cdot \mathcal{G}$ transport driven by TG turbulence. $\mathcal{G}$ equals zero below $(\nabla T_e/T_e)_c$ and increases strongly above it whereas ξ_{TG} describes the transport magnitude driven by the unstable modes. The threshold is predicted to vary with plasma parameters: $\nabla n_e/n_e$ and fraction of trapped electrons for TEMs [11], T_e/T_i, effective ion charge Z_{eff} and ratio of magnetic shear to safety factor $\hat{s}/q$ for ETG [16,17]. Finally the gyro-Bohm behavior is provided by $T^{3/2}$, a positive dependence of χ_e upon T_e which leads to an increase of stiffness with temperature. For simplicity we use the absolute value of ∇T_e and ∇n_e which are, as usual, negative in these experiments.

Recent specific experiments with electron cyclotron heating in ASDEX Upgrade showed that the T_e profiles are stiff which is provided by a change in heat diffusivity [18]. In this Letter we present results on experimental properties of the electron heat transport. The experiments were carried out in the ASDEX Upgrade divertor tokamak (major radius $R_0 = 1.65$ m, minor radius $a = 0.5$ m, elongation $\kappa \approx 1.6$). We used low density L modes ($\bar{n}_e \approx 2 \times 10^{19} m^{-3}$) with electron-cyclotron heating (ECH), providing conditions in which the electrons are hot and decoupled from the cold ions. Therefore the results can be ascribed specifically to the electrons. The ECH is provided by four systems (2 sec, 0.5 MW each) at the 2nd harmonic X mode ensuring here 100% single-pass absorption and can be modulated in power to study transport by analyzing the propagation of heat pulses. The deposition of the narrowly focused Gaussian beams ($w/a < 0.05$) can be varied independently by mirrors to fulfill the experimental requirements. The essential diagnostic here is the electron-cyclotron emission (ECE) heterodyne radiometer providing T_e profiles with 60 channels in space covering the whole plasma radius with a radial resolution of about 1 cm and a bandwidth of 32 kHz. The calibration yields a precision on T_e of $\pm 10\%$.

We first concentrate on experiments with ECH power up to 1.6 MW deposited in the center. The T_e profiles, averaged over several sawteeth, are plotted in Fig. 1 versus major radius in the outboard midplane $R - R_{\mathrm{mag}}$, where the diagnostic is located. R_{mag} is the radius of the magnetic axis. Following Refs. [1,4,7] and the expectation from stiff profiles, we use a semilog presentation. The lines

 0031-9007/01/86(24)/5498(4)$15.00

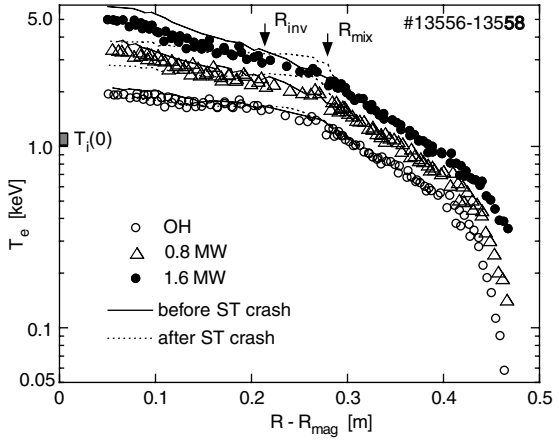

FIG. 1. T_e profiles for central ECH (ohmic, 0.8 and 1.6 MW) versus plasma radius in the LFS equatorial plane. The range of the central ion temperature is also indicated.

illustrate for each case the profiles just before and just after a sawtooth crash, the latter indicating the mixing radius R_{mix}. Note that the perturbations present outside R_{inv} just after a crash disappear very quickly and have no influence on the averaged profiles. The time-averaged heat flux caused by the sawtooth crashes represents 10% of the total heat flux at R_{inv}.

The averaged T_e profiles have a similar shape and are shifted according to their edge temperature, as expected from stiff profiles described above. In particular, a region from $R - R_{\mathrm{mag}} \approx 0.25$ m to $R - R_{\mathrm{mag}} \approx 0.43$ m, where their slope $\nabla T_e/T_e$ is the same can be clearly identified. This is the stiff region. In the center ($0.25 < R - R_{\mathrm{mag}}$) the slope changes and is different for each power. Note that the knee caused by the slope change is clearly outside R_{inv}, but not far from R_{mix}. We interpret the knee as the inner boundary of the stiff region. Inside the position of the knee, transport seems to be determined by other mechanisms. It is for instance possible that, due to the flat q profile (weak shear) produced by the sawteeth inside R_{mix}, turbulence modes are partly stabilized. In addition, sawteeth may also limit the T_e profile. Therefore we do not address this inner part of the plasma in the rest of the paper. Outside of the stiff region the profile slope gradually increases with radius. This deviation is stronger at low temperature (OH and 0.8 MW cases) and starts at smaller values of $R - R_{\mathrm{mag}}$ than at high temperatures (1.6 MW case). It seems to occur for T_e values below $\approx$700 eV, as also observed earlier in TFTR [4]. Finally, neutral particle analysis, quite reliable at such low densities, indicates that the central ion temperature remains almost constant around 1 keV in these discharges and therefore much lower than T_e.

The electron density profile reacts to the ECH power as indicated by Fig. 2. The density profile clearly flattens and broadens at high ECH power indicating an increase of particle transport linked with the electron heat transport. This observation suggests that electron turbulence causing heat transport may also affect particle transport. It will be

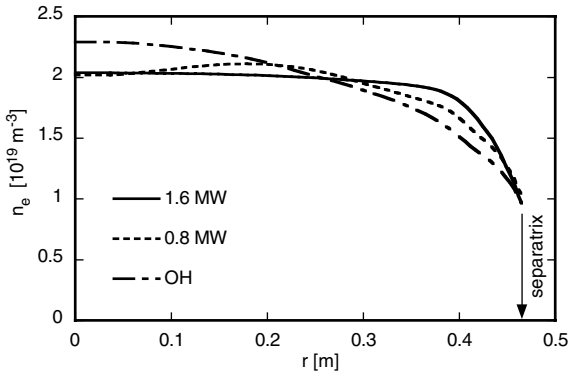

FIG. 2. Profiles of the electron density corresponding to the cases of Fig. 1.

discussed elsewhere [19]. As $\nabla T_e/T_e$ is a key parameter in these investigations on heat transport, it is useful to obtain experimentally this quantity with accuracy. For this purpose we shifted the plasma radially, by about 4 cm, during steady-state phases.

This method is similar to the "jogs" made in TFTR [20] with the difference that in our experiments the plasma movement was not fast and the measurement made in steady-state phases prior and after the displacement.

This allows one to measure ∇T_e for each single ECE channel using the relative displacement of the plasma which is known with accuracy ($\approx$5%) and the absolute ∇T_e is measured with a higher precision than done usually by fitting the profile. It is pointed out that, in our case, the calibration of the ECE diagnostic, which consists of one factor for each channel, cancels in the ratio $\nabla T_e/T_e$, providing this quantity with an accuracy of about 5%.

The results are given in Fig. 3, restricted to the region outside of R_{inv}, as mentioned above. Note the excellent alignment of the points provided by the method, without any smoothing or fitting of the T_e profiles. The stiff region where $\nabla T_e/T_e$ depends weakly on radius and the outer region where $\nabla T_e/T_e$ increases strongly with radius are clearly seen. In the stiff region, $\nabla T_e/T_e$ almost does not depend on the ECH power, whereas the curves for the three powers clearly separate in the outer region. The stiff

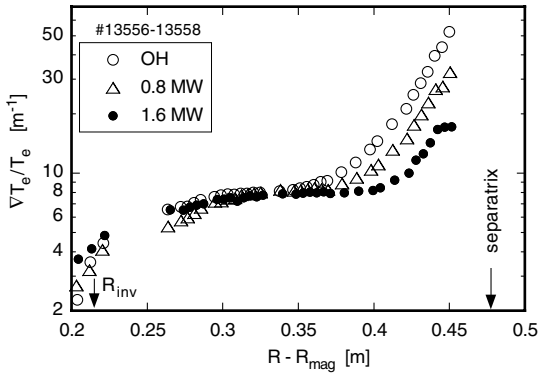

FIG. 3. $\nabla T_e/T_e$ versus plasma radius in the LFS equatorial plane for the cases of Fig. 1.

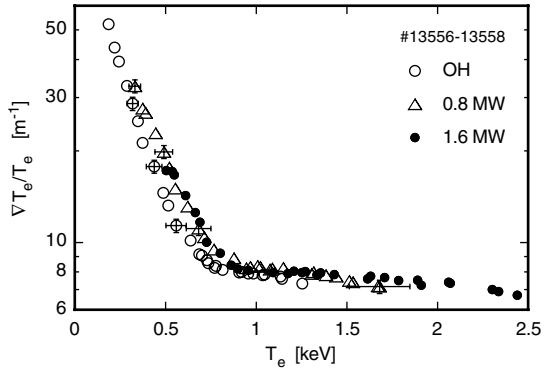

FIG. 4. $\nabla T_e/T_e$ versus T_e for the data of Fig. 3.

region extends further towards the edge with increasing power. Plotting $\nabla T_e/T_e$ versus T_e instead of radius, as in Fig. 4, suggests that T_e is a key parameter. The points for the three power levels coincide quite well over the whole temperature range, even at low temperature in the edge region.

Theory indicates that the threshold for ETG [17] and TEM [11] modes increases at large values of $\nabla n_e/n_e$, in our case above 5 m^{-1}. This quantity is large only at the plasma edge in our case, as shown by Fig. 2. The local values of $\nabla n_e/n_e$ plotted in Fig. 5 versus T_e for comparison with Fig. 4 clearly indicate that the changes in $\nabla n_e/n_e$ for the three cases do not coincide with the increase of $\nabla T_e/T_e$ in the low temperature region. We believe therefore that this is not the main cause for the high values of $\nabla T_e/T_e$ in the edge region and that the low temperature is more likely the reason. Discharges at 0.6 MA with overall lower temperature [18] support this hypothesis.

The good quality of our $\nabla T_e/T_e$ data allows one to calculate by power balance $\chi_e/T_e^{3/2}$ with precision. According to Eq. (1), this quantity is expected to exhibit a threshold in $\nabla T_e/T_e$ and the three cases should show the best agreement for the $T_e^{3/2}$ normalization. The experimental results are presented in Fig. 6. In this figure, going from low to high values of $\nabla T_e/T_e$ corresponds to a radial excursion from $R_{\rm inv}$ to the edge at $R - R_{\rm mag} = 0.43$ m.

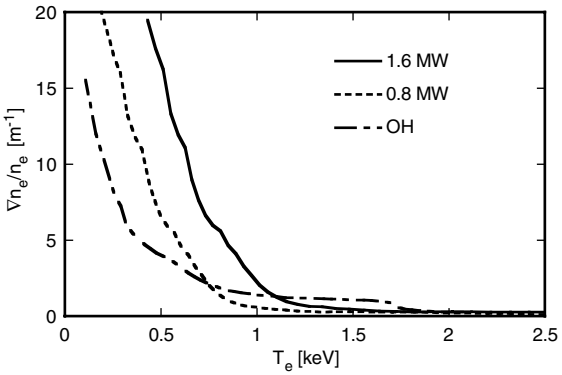

FIG. 5. $\nabla n_e/n_e$ versus T_e corresponding to Fig. 4.

These three cases, which correspond to a variation in heat flux and T_e of about a factor of 3, indeed exhibit the expected properties: they coincide in the central part within the error bars, have the same threshold as well as the same slope above the threshold, and saturate for larger values of $\nabla T_e/T_e$. Other normalizations than $T_e^{3/2}$ yield less good agreement between the data. Note that the data are not plotted at constant temperature, as one would do following Eq. (1). Therefore, the roll-off is not attributed to the saturation of the turbulence intensity at given T_e, but reflects the decrease of stiffness at low temperature as discussed previously. In Fig. 6 ∇T_e was calculated with respect to $R - R_{\rm mag}$, as above. We believe that, due to its ballooning character, turbulence and therefore transport processes are determined by $\nabla T_e/T_e$ on the low field side of the T_e profile. The effective heat transport is of course averaged over the flux surfaces by fast parallel equilibration. Using ∇T_e averaged over the flux surfaces, as generally done for power balance analysis, yields a nonmonotonic S-shaped behavior above the threshold, shown by the diamonds in Fig. 6.

A detailed comparison of these results with turbulence calculation is out of the scope of this experimental work, but comparison with formulas for $(\nabla T_e/T_e)_c$ for TEM [11] and ETG [17] was made. The threshold for TEM is clearly a factor of 2 to 3 below our measurements, whereas that for ETG exhibits a better agreement. The TEM instability is perhaps too weak under the present conditions to keep the profiles close to its threshold. Whether the ETG (with streamers) are limiting the profiles cannot be answered yet. The weak variation of $(\nabla T_e/T_e)_c$ with R and with heating power in the stiff region could be due, for ETG, to a compensation between the dependencies upon T_e/T_i and $\hat{s}/q$, as suggested in Ref. [17].

Modulation of the ECH power allows one to study the so-called transient transport, yielding the heat pulse diffusivity $\chi_e^{\rm HP}$. This value is per nature different from

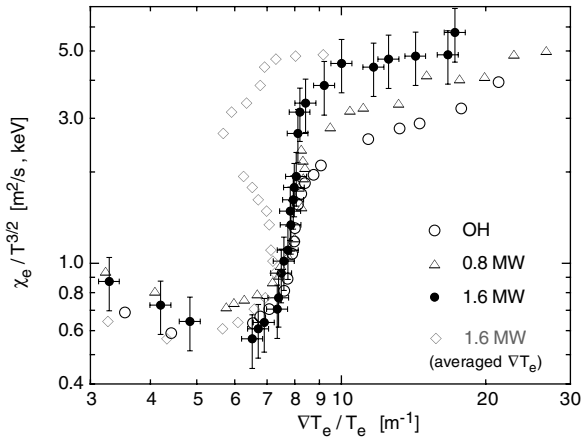

FIG. 6. Data points for χ_e^{PB} normalized by $T_e^{3/2}$ versus $\nabla T_e/T_e$ for the discharges of the previous figures.

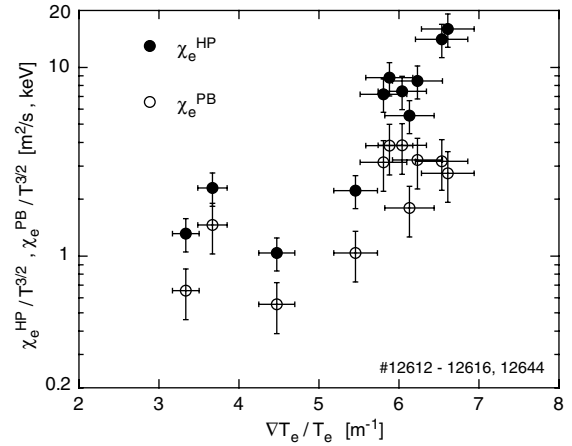

FIG. 7. χ_e^{HP} and χ_e^{PB} measured at $\rho = 0.6$ plotted versus $\nabla T_e/T_e$. The uncertainties on $\nabla T_e/T_e$ are relative as this quantity is deduced from the same 2 ECE channels for all the points. The absolute (systematic) error is larger (≈30%) but only causes a translation of all the points and therefore does not change the essence of the results.

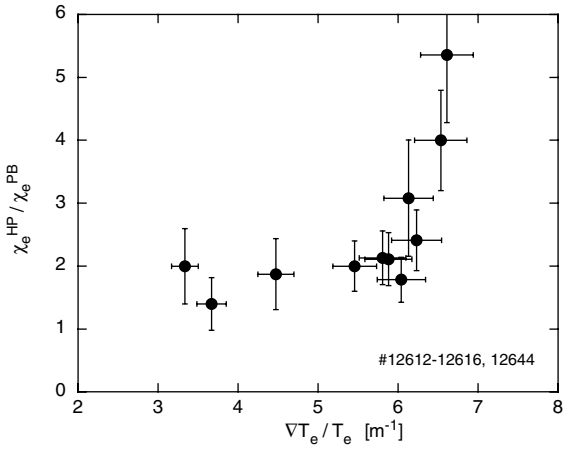

FIG. 8. Stiffness factor $\chi_e^{\mathrm{HP}}/\chi_e^{\mathrm{PB}}$ measured at $\rho = 0.6$ plotted versus $\nabla T_e/T_e$, from the data of Fig. 7.

the usual diffusivity deduced from power balance analysis χ_e^{PB}, because χ_e^{HP} is the slope of the heat flux versus $n_e \cdot \nabla T$, at the time-averaged working point [21]. In our analysis we calculate χ_e^{HP} from the standard method based on the Fourier transform of the T_e perturbation and slab model, as described in Ref. [21], applying the corrections for cylindrical geometry and density gradient effects according to Ref. [22]. The ratio $\chi_e^{\mathrm{HP}}/\chi_e^{\mathrm{PB}}$ is called stiffness factor: if it is close to unity the profiles are not stiff, but become stiffer as it increases. We applied the modulation technique to investigate experimentally the response of χ_e^{HP} to changes in $\nabla T_e/T_e$.

For this purpose we launched heat pulses from the plasma edge towards the center by modulating one gyrotron depositing at $\rho \approx 0.9$ and analyzed their propagation in a narrow region around $\rho = 0.6$, where ρ is the usual normalized toroidal flux radius. The sawteeth are small and do not perturb this experiment. We changed $\nabla T_e/T_e$ in the region of analysis by varying the CW power of other gyrotrons having their absorption layer at $\rho_{\mathrm{dep}} = 0.5$ or $\rho_{\mathrm{dep}} = 0.7$. In the configuration with $\rho_{\mathrm{dep}} = 0.5$ the measurement at $\rho \approx 0.6$ is placed in the stiff region of the profile, whereas in the case $\rho_{\mathrm{dep}} = 0.7$ it is in the region where the profile is driven to values below $(\nabla T_e/T_e)_c$. The results, given in Fig. 7, show a threshold in $\nabla T_e/T_e$ with a strong increase of χ_e^{HP} by about 1 order of magnitude for a small variation in $\nabla T_e/T_e$, whereas the variation of χ_e^{PB} is smaller. The corresponding stiffness factor shown in Fig. 8 clearly exhibits a strong increase above $(\nabla T_e/T_e)_c \approx 6\ \mathrm{m}^{-1}$, demonstrating without ambiguity the transition from nonstiff to stiff T_e profiles when crossing $(\nabla T_e/T_e)_c$.

In summary, our investigations provide detailed experimental data on the electron heat transport from both steady-state and modulation studies with ECH. The existence of a threshold $(\nabla T_e/T_e)_c$ is clearly demonstrated. The precise measurements of $\nabla T_e/T_e$ show a weak increase of this quantity with radius in the confinement zone and a strong increase close to edge, attributed to a loss of stiffness at low temperature.

Fruitful discussions with X. Garbet, F. Jenko, A. G. Peeters, and J. Weiland are warmly acknowledged, as well as the excellent support of the ECRH and ASDEX Upgrade Teams.

[1] R. Goldston *et al.,* in *Proceedings of the 11th IAEA Conference, Kyoto, 1986* [Plasma Phys. Controlled Nucl. Fusion Res. **3**, 75 (1987)].
[2] V. Alikaev *et al.,* in *Proceedings of the 11th IAEA Conference, Kyoto, 1986* [Plasma Phys. Controlled Nucl. Fusion Res. **3**, 111 (1987)].
[3] F. Wagner *et al.,* Phys. Rev. Lett. **56**, 2187 (1986).
[4] G. Taylor *et al.,* Nucl. Fusion **29**, 3 (1989).
[5] T. Luce *et al.,* Phys. Rev. Lett. **68**, 52 (1992).
[6] C. Petty *et al.,* Nucl. Fusion **34**, 121 (1994).
[7] W. Suttrop *et al.,* Plasma Phys. Controlled Fusion **39**, 2051 (1997).
[8] P. Gohil *et al.,* Nucl. Fusion **38**, 425 (1998).
[9] L. D. Horton *et al.,* Plasma Phys. Controlled Fusion **41**, B329 (1999).
[10] J. Weiland *et al.,* Nucl. Fusion **29**, 1810 (1989).
[11] H. Nordman *et al.,* Nucl. Fusion **30**, 983 (1990).
[12] J. Nilsson *et al.,* Nucl. Fusion **35**, 497 (1995).
[13] A. Dimits *et al.,* Phys. Plasmas **7**, 969 (2000).
[14] F. Jenko *et al.,* Phys. Plasmas **7**, 1904 (2000).
[15] W. Dorland *et al.,* Phys. Rev. Lett. **85**, 5579 (2000).
[16] W. Horton *et al.,* Phys. Plasmas **7**, 1494 (2000).
[17] F. Jenko *et al.,* Phys. Plasmas (to be published).
[18] F. Ryter *et al.,* Phys. Rev. Lett. **86**, 2325 (2001).
[19] J. Stober *et al.* (to be published).
[20] M. Zarnstorff *et al.,* in *Proceedings of the Workshop on Local Transport Studies in Fusion Plasmas, Varenna, 1993* (Societa Italiana di Fisica, Bologna, 1994), p. 257.
[21] N. J. Lopes Cardozo, Plasma Phys. Controlled Fusion **37**, 799 (1995).
[22] A. Jacchia *et al.,* Phys. Fluids B **3**, 3033 (1991).